JAERI-Research
95-089

NUMERICAL PREDICTION OF TURBULENT HEAT TRANSFER AUGMENTATION IN AN ANNULAR FUEL CHANNEL WITH TWO-DIMENSIONAL SQUARE RIBS

January 1996

Kazuyuki TAKASE

日本原子力研究所
Japan Atomic Energy Research Institute

本レポートは，日本原子力研究所が不定期に公刊している研究報告書です。
入手の問合わせは，日本原子力研究所技術情報部情報資料課（〒319-11 茨城県那珂郡東海村）あて，お申し越しください。なお，このほかに財団法人原子力弘済会資料センター（〒319-11 茨城県那珂郡東海村日本原子力研究所内）で複写による実費頒布をおこなっております。

This report is issued irregularly.
Inquiries about availability of the reports should be addressed to Information Division, Department of Technical Information, Japan Atomic Energy Research Institute, Tokai-mura, Naka-gun, Ibaraki-ken 319-11, Japan.

編集兼発行　日本原子力研究所
印　　刷　㈱原子力資料サービス

JAERI－Research 95－089

Numerical Prediction of Turbulent Heat Transfer Augmentation in an Annular Fuel Channel with Two-dimensional Square Ribs

Kazuyuki TAKASE

Department of High Temperature Engineering
Tokai Research Establishment
Japan Atomic Energy Research Institute
Tokai-mura, Naka-gun, Ibaraki-ken

(Received December 11, 1995)

The square-ribbed fuel rod for high temperature gas-cooled reactors was developed in order to enhance the turbulent heat transfer in comparison with the standard fuel rod. To evaluate the heat transfer performance of the square-ribbed fuel rod, the turbulent heat transfer coefficients in an annular fuel channel with repeated two-dimensional square ribs were analyzed numerically on a fully developed incompressible flow using the k - ε turbulence model and the two-dimensional axisymmetrical coordinate system. Numerical analyses were carried out for a range of Reynolds numbers from 3000 to 20000 and ratios of square-rib pitch to height of 10, 20 and 40, respectively. The predicted values of the heat transfer coefficients agreed within an error of 10% for the square-rib pitch to height ratio of 10, 20% for 20 and 25% for 40, respectively, with the heat transfer empirical correlations obtained from the experimental data. It was concluded by the present study that the effect of the heat transfer augmentation by square ribs could be predicted sufficiently by the present numerical simulations and also a part of its mechanism could be explained by means of the change in the turbulence kinematic energy distribution along the flow direction

Keywords: Convective Heat Transfer, Numerical Analysis, Square-ribbed Annular Channels, Fully-developed Turbulent Flows, The k- ε Turbulence Model, Heat Transfer Augmentation

2次元矩形突起を有する環状燃料チャンネル内の乱流伝熱促進に関する数値予測

日本原子力研究所東海研究所高温工学部
高瀬　和之

（1995年12月11日受理）

高温ガス炉用標準燃料棒よりも乱流熱伝達率を向上させるために，矩形突起付き燃料棒の開発を行った。この矩形突起付き燃料棒の伝熱性能を評価するために，2次元の矩形突起を有する環状燃料チャンネル内の乱流熱伝達率を，k-ε乱流モデルと2次元軸対称座標系を使って十分に発達した非圧縮性流体に対して数値的に解析した。数値解析は，3000から20000のレイノルズ数範囲に対して，矩形突起のピッチと高さの比が10，20，40の3つの場合について行った。熱伝達率の予測値は，矩形突起付き燃料棒による実験データから求めた熱伝達相関式に対して，矩形突起のピッチと高さの比が10，20，40の場合にそれぞれ10%，20%及び25%以内の誤差で一致した。本研究により，矩形突起による伝熱促進効果は本数値シミュレーションによって十分予測できるとともに，そのメカニズムの一部は乱流エネルギー分布の流れ方向変化から良く説明できることが明らかになった。

東海研究所：〒319-11　茨城県那珂郡東海村白方白根2-4

Contents

目　　次

1. INTRODUCTION

Japan Atomic Energy Research Institute (JAERI) has been constructing a High Temperature Engineering Test Reactor (HTTR) so as to establish and upgrade technology of the very high temperature gas-cooled reactor and promote innovative high temperature research. HTTR is a helium-cooled, graphite-moderated reactor with a core inlet temperature of 395°C, maximum core outlet temperature of 950°C, pressure of 4 MPa, thermal power of 30 MW, and average power density of 2.5MW/m^3.

The pressure vessel of HTTR as shown in Fig. 1 has a height of 13.2 m and a diameter of 5.5 m, and contains the active core, permanent and replaceable reflectors, core support structure and core restraint mechanism. The active core consists of 30 fuel columns and 7 control-rod guide columns, each of which is composed of 5 hexagonal graphite blocks stacked vertically. The dimension of the graphite block is 360 mm in width across flats and 580 mm in height. Figure 2 shows the fuel element consisted of the graphite block and 33 fuel holes. A standard fuel rod with spacer ribs on its outer surface is inserted into each fuel hole. Helium gas flows downward through annular channels between the fuel hole with a diameter of 41 mm and the fuel rod with an external diameter of 34 mm. The author has already investigated experimentally (Takase, et al., 1986, 1990) and numerically [(Takase, 1995), (Takase and Akino, 1995)] the thermal-hydraulic performance of the standard fuel rod under the same helium gas conditions as the HTTR operation to obtain necessary data to design the HTTR core.

Then, the development of high heat flux fuel rods began to increase the power density of the HTTR core. A square-ribbed fuel rod was designed as one of several high heat flux fuel rods and a lot of very small square ribs on its outer surface. Rib-roughened surfaces are often used to enhance the convective heat transfer coefficient for high heat flux applications. Following researchers studied on the heat transfer coefficients augmented by the square ribs in flow channels. Maubach (1972) investigated the pressure drop in an annular duct with square ribs under isothermal flow condition. Dalle Donne and Meyer (1977) examined the turbulent heat transfer coefficients of fuel rods with square ribs under the condition of high heat flux from the inner wall of an annular passage, so that they derived a heat transfer empirical correlation for various ratios of pitch to height of the square rib. Han et al. (1978) investigated the effects of rib shape (i.e., round, rectangle and triangle), attack angle to the flow direction and ratio of rib pitch to height regarding turbulent heat transfer in a rectangular duct. On the other hand, numerical calculations for heated flow over a couple of ribs were carried out by Lee et al. (1988) for an annular duct with ribbed inner wall, Acharya et al. (1993) for a rectangular duct with ribbed-lower wall and Liou et al. (1991) and Chang and Mills (1993) for rectangular channels with ribbed upper and lower walls, respectively.

However, their experimental and numerical conditions, such as temperature, pressure and Reynolds number (Re) were different from the HTTR operation. In particular, the previous studies were conducted in a region of $Re \geq 10000$, however, the HTTR core is operated in a

region of *Re* from 3000 to less than 10000. From the viewpoint of the nuclear reactor safety, it is very risky to estimate the heat transfer performance of the square-ribbed fuel rod from the results of previous work.

Therefore, experiments were carried out to verify the thermal-hydraulic performance and long-term durability of the square-ribbed fuel rod under helium gas conditions of high temperature and pressure by Takase et al. (1991, 1993). However, it was impossible to obtain detailed information, such as local velocity, temperature and heat transfer coefficient, from these experimental results. In addition, it was difficult to discuss the mechanism of heat transfer augmentation by the square ribs. For these reasons, numerical analyses were undertaken to predict the turbulent heat transfer coefficients in the square-ribbed fuel channel with different ratios of square-rib pitch to height and carry out the design study for the high heat flux fuel rods. This paper describes the results of numerical analyses and comparison of the predictions with the experimental correlations, regarding the heat transfer augmentation in the annular fuel channel with two-dimensional square ribs.

2. SQUARE-RIBBED FUEL ROD

The square-ribbed fuel rod has almost the same configuration as the standard fuel rod except for the surface form. The standard fuel rod, as shown in Fig. 2, has nine spacer ribs on its smooth outer surface to keep the concentricity of the annulus. In addition, the square-ribbed fuel rod has very small two-dimensional square ribs on the outer surface to improve the convective turbulent heat transfer.

The simulated square-ribbed fuel rod used in the experiment is an electric heater with a maximum electric power of 70 kW with uniform axial heat flux distribution. It is composed of seven sub-rods, in which each sub-rod is connected axially. The sub-rod is 570 mm in length, 505~520 mm in artificial roughness length and 34 mm in diameter (*Di*) as shown in Fig. 3. Three kinds of the simulated square-ribbed fuel rods with different ratios of square-rib pitch to height were used in the experiment. As for each fuel rod, the dimensions of the square rib are 0.5 mm in height (*h*) and 0.5 mm in width (*w*) but the rib pitch (*p*) is set at 5, 10 and 20 mm; the ratios of square-rib pitch to height (*p/h*) are 10, 20 and 40, respectively. According to prior studies on the heat transfer augmentation by means of roughness, the turbulent heat transfer indicated the most improvement when *p/h* was nearly equal to 10. The *p/h* ratio was varied so as to investigate the effect of the square-rib arrangement for the turbulent heat transfer under the present annular channel conditions. Each rib was manufactured within a tolerance of ±0.05 mm. In the present study, an inner diameter (*Di*) of the annulus was defined as a diameter of 34 mm between the base positions of the square rib, an outer diameter (*Do*) was 41 mm. A hydraulic diameter (*De*) was 7 mm and then helium gas flowed downward in a very narrow annular channel. Furthermore, small trapezoidal spacer ribs were positioned at the top and

region of *Re* from 3000 to less than 10000. From the viewpoint of the nuclear reactor safety, it is very risky to estimate the heat transfer performance of the square-ribbed fuel rod from the results of previous work.

Therefore, experiments were carried out to verify the thermal-hydraulic performance and long-term durability of the square-ribbed fuel rod under helium gas conditions of high temperature and pressure by Takase et al. (1991, 1993). However, it was impossible to obtain detailed information, such as local velocity, temperature and heat transfer coefficient, from these experimental results. In addition, it was difficult to discuss the mechanism of heat transfer augmentation by the square ribs. For these reasons, numerical analyses were undertaken to predict the turbulent heat transfer coefficients in the square-ribbed fuel channel with different ratios of square-rib pitch to height and carry out the design study for the high heat flux fuel rods. This paper describes the results of numerical analyses and comparison of the predictions with the experimental correlations, regarding the heat transfer augmentation in the annular fuel channel with two-dimensional square ribs.

2. SQUARE-RIBBED FUEL ROD

The square-ribbed fuel rod has almost the same configuration as the standard fuel rod except for the surface form. The standard fuel rod, as shown in Fig. 2, has nine spacer ribs on its smooth outer surface to keep the concentricity of the annulus. In addition, the square-ribbed fuel rod has very small two-dimensional square ribs on the outer surface to improve the convective turbulent heat transfer.

The simulated square-ribbed fuel rod used in the experiment is an electric heater with a maximum electric power of 70 kW with uniform axial heat flux distribution. It is composed of seven sub-rods, in which each sub-rod is connected axially. The sub-rod is 570 mm in length, 505~520 mm in artificial roughness length and 34 mm in diameter (Di) as shown in Fig. 3. Three kinds of the simulated square-ribbed fuel rods with different ratios of square-rib pitch to height were used in the experiment. As for each fuel rod, the dimensions of the square rib are 0.5 mm in height (h) and 0.5 mm in width (w) but the rib pitch (p) is set at 5, 10 and 20 mm; the ratios of square-rib pitch to height (p/h) are 10, 20 and 40, respectively. According to prior studies on the heat transfer augmentation by means of roughness, the turbulent heat transfer indicated the most improvement when p/h was nearly equal to 10. The p/h ratio was varied so as to investigate the effect of the square-rib arrangement for the turbulent heat transfer under the present annular channel conditions. Each rib was manufactured within a tolerance of ±0.05 mm. In the present study, an inner diameter (Di) of the annulus was defined as a diameter of 34 mm between the base positions of the square rib, an outer diameter (Do) was 41 mm. A hydraulic diameter (De) was 7 mm and then helium gas flowed downward in a very narrow annular channel. Furthermore, small trapezoidal spacer ribs were positioned at the top and

bottom locations of each sub-rod to keep axially the concentricity of the annular channel. The tolerance between *Do* and the tip diameter of the spacer ribs is less than 0.3 mm. There is a full description in the Ref. (Takase, 1995) regarding the experimental facility in which the simulated square-ribbed fuel rods were carried out.

3. NUMERICAL ANALYSIS

3.1. Governing equations

The continuity, Reynolds averaged Navier-Stokes and energy equations in conjunction with the eddy viscosity concept under the incompressible flow can be written using a two-dimensional axisymmetrical coordinate as:

Continuity

$$\frac{\partial}{\partial x}(\rho u)+\frac{1}{r}\frac{\partial}{\partial r}(r\rho v)=0 \tag{1}$$

Momentum of x direction

$$\frac{\partial}{\partial x}(\rho uu)+\frac{1}{r}\frac{\partial}{\partial r}(r\rho uv)=-\frac{\partial P_p}{\partial x}+\beta+\frac{\partial}{\partial x}\left[\mu_{eff}\left(2\frac{\partial u}{\partial x}\right)\right] +\frac{1}{r}\frac{\partial}{\partial r}\left[r\mu_{eff}\left(\frac{\partial v}{\partial x}+\frac{\partial u}{\partial r}\right)\right]-\frac{2}{3}\frac{\partial(\rho k)}{\partial x} \tag{2}$$

Momentum of r direction

$$\frac{\partial}{\partial x}(\rho uv)+\frac{1}{r}\frac{\partial}{\partial r}(r\rho vv)=-\frac{\partial P_p}{\partial r}+\frac{\partial}{\partial x}\left[\mu_{eff}\left(\frac{\partial v}{\partial x}+\frac{\partial u}{\partial r}\right)\right] +\frac{1}{r}\frac{\partial}{\partial r}\left[r\mu_{eff}\left(2\frac{\partial v}{\partial r}\right)\right]-2\mu_{eff}\frac{v}{r^2}-\frac{2}{3}\frac{\partial(\rho k)}{\partial r} \tag{3}$$

Energy

$$\frac{\partial}{\partial x}(\rho uT)+\frac{1}{r}\frac{\partial}{\partial r}(r\rho vT)=-\frac{\partial}{\partial x}\left(\frac{\mu_{eff}}{Pr_{eff}}\frac{\partial T}{\partial x}\right)+\frac{1}{r}\frac{\partial}{\partial r}\left(r\frac{\mu_{eff}}{Pr_{eff}}\frac{\partial T}{\partial r}\right) \tag{4}$$

where the effective viscosity (μ_{eff}) and the effective Prandtl number (Pr_{eff},) are given by

$$\mu_{eff}=\mu_t+\mu,\quad \mu_t=C_\mu\rho k^2/\varepsilon,\quad Pr_{eff}=\mu/Pr+\mu_t/Pr_t \tag{5}$$

In addition, the pressure (P) in case of a periodic fully developed flow is separated into two parts as proposed by Patankar et al. (1977):

bottom locations of each sub-rod to keep axially the concentricity of the annular channel. The tolerance between *Do* and the tip diameter of the spacer ribs is less than 0.3 mm. There is a full description in the Ref. (Takase, 1995) regarding the experimental facility in which the simulated square-ribbed fuel rods were carried out.

3. NUMERICAL ANALYSIS

3.1. Governing equations

The continuity, Reynolds averaged Navier-Stokes and energy equations in conjunction with the eddy viscosity concept under the incompressible flow can be written using a two-dimensional axisymmetrical coordinate as:

Continuity

$$\frac{\partial}{\partial x}(\rho u)+\frac{1}{r}\frac{\partial}{\partial r}(r\rho v)=0 \tag{1}$$

Momentum of x direction

$$\frac{\partial}{\partial x}(\rho uu)+\frac{1}{r}\frac{\partial}{\partial r}(r\rho uv)=-\frac{\partial P_p}{\partial x}+\beta+\frac{\partial}{\partial x}\left[\mu_{eff}\left(2\frac{\partial u}{\partial x}\right)\right] +\frac{1}{r}\frac{\partial}{\partial r}\left[r\mu_{eff}\left(\frac{\partial v}{\partial x}+\frac{\partial u}{\partial r}\right)\right]-\frac{2}{3}\frac{\partial(\rho k)}{\partial x} \tag{2}$$

Momentum of r direction

$$\frac{\partial}{\partial x}(\rho uv)+\frac{1}{r}\frac{\partial}{\partial r}(r\rho vv)=-\frac{\partial P_p}{\partial r}+\frac{\partial}{\partial x}\left[\mu_{eff}\left(\frac{\partial v}{\partial x}+\frac{\partial u}{\partial r}\right)\right] +\frac{1}{r}\frac{\partial}{\partial r}\left[r\mu_{eff}\left(2\frac{\partial v}{\partial r}\right)\right]-2\mu_{eff}\frac{v}{r^2}-\frac{2}{3}\frac{\partial(\rho k)}{\partial r} \tag{3}$$

Energy

$$\frac{\partial}{\partial x}(\rho uT)+\frac{1}{r}\frac{\partial}{\partial r}(r\rho vT)=-\frac{\partial}{\partial x}\left(\frac{\mu_{eff}}{Pr_{eff}}\frac{\partial T}{\partial x}\right)+\frac{1}{r}\frac{\partial}{\partial r}\left(r\frac{\mu_{eff}}{Pr_{eff}}\frac{\partial T}{\partial r}\right) \tag{4}$$

where the effective viscosity (μ_{eff}) and the effective Prandtl number (Pr_{eff},) are given by

$$\mu_{eff}=\mu_t+\mu,\quad \mu_t=C_\mu\rho k^2/\varepsilon,\quad Pr_{eff}=\mu/Pr+\mu_t/Pr_t \tag{5}$$

In addition, the pressure (P) in case of a periodic fully developed flow is separated into two parts as proposed by Patankar et al. (1977):

$$P(x, r) = -\beta\ x + P_P(x,r) \tag{6}$$

Where, $P_p(x, r)$ represents the periodic parts of the pressure and β represents the pressure drop parameter during a one periodic length, respectively.

Turbulent kinematic energy (k) and its dissipation rate (ε) are computed from the two equation standard k-ε model of Jones and Launder (1972):

$$\frac{\partial}{\partial x}(\rho u k) + \frac{1}{r}\frac{\partial}{\partial r}(r\rho v k) = \frac{\partial}{\partial x}\left(\frac{\mu_t}{\sigma_k}\frac{\partial k}{\partial x}\right) + \frac{1}{r}\frac{\partial}{\partial r}\left(r\frac{\mu_t}{\sigma_k}\frac{\partial k}{\partial r}\right) + P_k - \rho\varepsilon \tag{7}$$

$$\frac{\partial}{\partial x}(\rho u \varepsilon) + \frac{1}{r}\frac{\partial}{\partial r}(r\rho v \varepsilon) = \frac{\partial}{\partial x}\left(\frac{\mu_t}{\sigma_\varepsilon}\frac{\partial \varepsilon}{\partial x}\right) + \frac{1}{r}\frac{\partial}{\partial r}\left(r\frac{\mu_t}{\sigma_\varepsilon}\frac{\partial \varepsilon}{\partial r}\right) + C_1\frac{\varepsilon}{k}P_k - C_2\frac{\varepsilon^2}{k} \tag{8}$$

P_k denotes the production rate of k which is obtained by :

$$P_k = \mu_t\left\{2\left[\left(\frac{\partial u}{\partial x}\right)^2 + \left(\frac{\partial v}{\partial r}\right)^2 + \left(\frac{v}{r}\right)^2\right] + \left(\frac{\partial v}{\partial x} + \frac{\partial u}{\partial r}\right)^2\right\} \tag{9}$$

The standard k-ε model constants (Jones and Launder, 1972) are applied:

$$C_\mu = 0.09,\ C_1 = 1.44,\ C_2 = 1.92,\ \sigma_k = 1.0,\ \sigma_\varepsilon = 1.3,\ Pr_t = 0.9. \tag{10}$$

It was reviewed from the previous experimental studies for flow over two rib roughness in a channel that the turbulent shear stress and degree of anisotropy between normal stresses were very sensitive to stream curvature. Therefore, it was expected that this sensitivity might be not reflected sufficiently in the numerical results because the k-ε model was essentially isotropic. However, past numerical analyses of Durst et al. (1988), Lee et al. (1988) and Liou et al. (1991) on turbulent flows in rib-roughened channels using the k-ε model have been relatively successful where a distance between a couple of square ribs is short and also fluid properties are supposed as constant. Therefore, the k-ε model was used to the present study.

3.2. Numerical conditions

Figure 4 shows an analytical model and the boundary conditions for the present numerical analysis. The computation was performed for a one pitch length between a couple of square ribs in the two-dimensional annular channel. The working fluid flows from the left to right over the square ribs.

The computational conditions were as followings: The fluid was helium gas with an initial temperature of 500°C and pressure of 4 MPa. The average *Re* at the channel inlet was varied from 3000 to 20000, and the inner wall heat flux on ABCDEF in Fig. 4 was also varied from

38 to 252 kW/m^2 corresponding to the variation of Re. The outer wall was insulated thermally and all heat conduction in walls were neglected. The radiation between the inner to outer walls was considered. The emissivities of 0.8 for graphite (Goldsmith et al., 1961) and 0.3 for Incolloy 800H (Makino et al., 1983) were given for the inner and outer wall in correspondence with the experimental condition. In addition, the constant thermophysical properties were assumed. Dimensions of H, h and w were 3.5, 0.5 and 0.5 mm, respectively. Three cases of computations were carried out for p/h=10, 20 and 40 under constant heat flux conditions. These computational grid point for each p/h was 56×42, 106×42 and 206×42 and distributed in a non-uniform manner with higher concentrations of the grids closer to the walls. Decisions for each grid number were based on the results of Acharya, et al. (1993).

3.3. Boundary conditions

Fluid velocities, u and v, were zero at the walls. To obtain a hydrodynamically fully developed velocity profile at the inlet section of the computational domain, periodic boundary conditions were set at the inlet and outlet sections. In the present study, the approach of Patankar et al. (1977) to the periodic boundary conditions was used to avoid the entrance region problems.

The wall function proposed by Launder and Spalding (1974), which was a log-law for y^+>11.6 and a linear-law for y^+≤11.6, was used to prescribe the boundary conditions along the channel walls. Here, y^+ denotes the dimensionless distance from the wall and is specified as:

$$y^+ = \frac{\rho u_p C_\mu^{1/4} k_p^{1/2}}{\mu} \tag{11}$$

In Eq. (11), the subscript p refers to the grid point adjacent to the wall. In addition, the wall shear stress is specified as:

$$\tau_w = \frac{\rho u_p C_\mu^{1/4} k_p^{1/2} \kappa}{\ln(Ey^+)} \tag{12}$$

Here, κ≅0.42 and E=9.0.

For the temperature boundary condition, the heat flux to the wall is derived from the thermal wall function (Launder and Spalding, 1974):

$$q_w = \frac{(T_w - T_p)\rho c_p C_\mu^{1/4} k_p^{1/2}}{Pr_t\left[\frac{1}{\kappa}\ln(Ey^+) + P_f\right]} \tag{13}$$

Where the empirical P_f function is specified as :

$$P_f = \frac{\pi/4}{\sin(\pi/4)}\left(\frac{A}{\kappa}\right)^{1/2}\left(\frac{Pr}{Pr_t}-1\right)\left(\frac{Pr_t}{Pr}\right)^{1/4} \tag{14}$$

3.4. Numerical procedure

The FLUENT, which was a thermal-hydraulic analysis code, was used in the present study. Its computational algorithm was based on the SIMPLE method proposed by Patankar (1980) and the control volume approach was adopted to solve the governing equations (1)~(4) and (7), (8) using a finite difference scheme. The convection and diffusion terms in the governing equations were discretized by using the power law and the central differencing schemes, respectively, and the discretized equations were solved using a line-by-line Tri-Diagonal Matrix Algorithm.

The criterion for the convergence of the numerical solution was based on the normalized residuals of each equation that was summed for all cells in the computational domain. The solutions were regarded as converged when these normalized residuals became less than 10^{-4} for all flow variables and 10^{-6} for the energy equation.

4. COMPUTATIONAL RESULTS AND DISCUSSION

To validate the calculation results of the turbulent heat transfer computed by the FLUENT code, the author first predicted the heat transfer experimental results of Hishida and Takase (1991). The local heat transfer coefficients on the heated surface were particularly measured on a ribbed lower wall with smooth upper and side walls under a fully-developed turbulent flow in a rectangular duct. The experimental conditions were as follows: The working fluid was air with atmospheric temperature and pressure; The channel dimensions were 907 mm in width and 95.5 mm in height; The rib dimensions were 11.5 mm in width and 10 mm in height; p/De=0.058; p/h=60; The constant heat flux was given for the lower wall in the channel including the rib surface; All channel walls except the lower wall were adiabatic; The Re at the inlet of measuring section in the channel was varied from 6000 to 10^5.

A comparison of the predicted heat transfer coefficients (α) with the experimental data for Re=6000 and 11000 are shown in Fig. 5. Here, square and circle symbols and dashed and solid lines represent the experimental data and the predicted values for Re=6000 and 11000, respectively. The predicted heat transfer coefficients were overestimated with the experimental data, however, an error between the experimental data and the predictions was less than 10% for Re=6000 and 4% for Re=11000, respectively. It was concluded from these results that the present numerical procedure could be applied sufficiently for a turbulent flow over repeated transverse square ribs.

Figure 6 represents the predicted axial velocity distribution along the flow direction between

$$P_f = \frac{\pi/4}{\sin(\pi/4)}\left(\frac{A}{\kappa}\right)^{1/2}\left(\frac{Pr}{Pr_t}-1\right)\left(\frac{Pr_t}{Pr}\right)^{1/4} \tag{14}$$

3.4. Numerical procedure

The FLUENT, which was a thermal-hydraulic analysis code, was used in the present study. Its computational algorithm was based on the SIMPLE method proposed by Patankar (1980) and the control volume approach was adopted to solve the governing equations (1)~(4) and (7), (8) using a finite difference scheme. The convection and diffusion terms in the governing equations were discretized by using the power law and the central differencing schemes, respectively, and the discretized equations were solved using a line-by-line Tri-Diagonal Matrix Algorithm.

The criterion for the convergence of the numerical solution was based on the normalized residuals of each equation that was summed for all cells in the computational domain. The solutions were regarded as converged when these normalized residuals became less than 10^{-4} for all flow variables and 10^{-6} for the energy equation.

4. COMPUTATIONAL RESULTS AND DISCUSSION

To validate the calculation results of the turbulent heat transfer computed by the FLUENT code, the author first predicted the heat transfer experimental results of Hishida and Takase (1991). The local heat transfer coefficients on the heated surface were particularly measured on a ribbed lower wall with smooth upper and side walls under a fully-developed turbulent flow in a rectangular duct. The experimental conditions were as follows: The working fluid was air with atmospheric temperature and pressure; The channel dimensions were 907 mm in width and 95.5 mm in height; The rib dimensions were 11.5 mm in width and 10 mm in height; p/De=0.058; p/h=60; The constant heat flux was given for the lower wall in the channel including the rib surface; All channel walls except the lower wall were adiabatic; The Re at the inlet of measuring section in the channel was varied from 6000 to 10^5.

A comparison of the predicted heat transfer coefficients (α) with the experimental data for Re=6000 and 11000 are shown in Fig. 5. Here, square and circle symbols and dashed and solid lines represent the experimental data and the predicted values for Re=6000 and 11000, respectively. The predicted heat transfer coefficients were overestimated with the experimental data, however, an error between the experimental data and the predictions was less than 10% for Re=6000 and 4% for Re=11000, respectively. It was concluded from these results that the present numerical procedure could be applied sufficiently for a turbulent flow over repeated transverse square ribs.

Figure 6 represents the predicted axial velocity distribution along the flow direction between

the inner and outer walls at p/h=10 and Re =5000. Here, r/H means the dimensionless radial distance from the inner to outer walls and x/h the dimensionless axial distance from the inlet to outlet sections. A maximum axial velocity is shown in the turbulent core region along the flow direction. On the other hand, a negative velocity appears in a region just behind the first rib. This implies the existence of recirculation. In the present study, the recirculation zone becomes larger as p/h increases. In addition, a small recirculation is predicted in upstream of the second rib and a very small counter-rotating vortex also takes place in the corner just after the first rib.

Corresponding to Fig. 6, the predicted radial velocity distribution along the flow direction between the inner and outer walls is shown in Fig. 7. A maximum radial velocity is observed at the upstream edge of the second rib. A next large velocity is seen at the downstream side of the first rib because the fluid flows upward due to recirculation. On the other hand, the radial velocity in a turbulent core region is almost equal to zero, and this denotes that the influence of the flow disturbance by the square ribs do not reach to the turbulent core region.

Figure 8 shows the radial distributions of the predicted axial velocity for each p/h at the middle position between a couple of square ribs at Re=5000. Here, the solid, broken and dashed lines present p/h=10, 20 and 40, respectively. The recirculation no longer exists. The maximum velocity appears at r/H=0.68 for p/h =10, 0.62 for 20 and 0.54 for 40. That is, the position of maximum velocity comes close to the inner wall as p/h increased.

Radial distributions of the predicted turbulence kinematic energy along the flow direction between a couple of square ribs at Re=5000 are shown in Fig. 9(a) for p/h=10 and Fig. 9(b) for p/h=40. In Fig. 9(a), the turbulence kinematic energy increases greatly near the square rib where a highly turbulent shear flow is generated by the square ribs, and its maximum value appears at the upstream edge of the rib where the flow impinges. On the other hand, the turbulence kinematic energy in Fig. 9(b) shows a higher value at the top of the first rib as same as that in Fig. 9(a), however, it decreases gradually along the flow direction and represents almost flat distributions near the inner wall region from the middle position between two square ribs. From these results, the following consideration can be derived: when p/h is smaller, the turbulence with large kinematic energy always exists from the top of the upstream rib to that of the downstream rib, and thus, the high heat transfer coefficient can be expected because large turbulence is produced. When p/h is larger, however, the large turbulence generated at the top of the upstream rib is reduced along the flow direction and disappears when it approaches the second rib. Therefore, it is considered that the heat transfer coefficients in the square-ribbed fuel channel with the larger p/h are lower than those with the smaller p/h.

Figure 10 represents a comparison of the predicted maximum turbulence kinematic energy at the middle position between the square ribs with Re when p/h=10, 20 and 40. Here, the solid, broken and dashed lines mean p/h=10, 20 and 40, respectively. The turbulence kinematic energy for each p/h varies as a straight line on the logarithmic scale and also its value is high as p/h decreases.

As an example of predicted temperature distributions, the predicted radial temperature profiles between the inner and outer walls with different ratios of x/h at p/h=10 and Re=5000 are shown in Fig. 11. Each line means a different axial location where x/h=0.5, 1, 5, 9 and 9.5, respectively. The predicted temperature increases suddenly on the inner wall and represents the highest value at x/h=0.5. From this result, it can be considered that a hot spot takes place at the vicinity of the base position just after the rib. On the other hand, the predicted temperature at each x/h indicates almost the same profile in the range of r/H >0.3.

Figure 12 shows the predicted inner wall temperature (T_w) distributions between the ribs with different ratios of p/h at Re=5000. Here, the solid, broken and dashed lines mean T_w distributions when p/h=10, 20 and 40, respectively. In addition, three kinds of longitudinal axes indicate the x/h ratios when p/h=10, 20 and 40, respectively. The T_w represents the maximum value at the downstream base of the rib and also the next larger value at the upstream base of the rib because the flow is stagnant at both locations where the recirculation is caused. On the other hand, T_w far from the base position of the rib decreases to a great extent. In general, the heat transfer coefficient is high where T_w is low. Therefore, it is expected for each p/h ratio that the best heat transfer coefficient can be seen at about x/h=5 where T_w indicates the minimum value.

Variations in the predicted local heat transfer coefficient (α) along the flow direction at Re=5000 are shown in Fig. 13(a) for p/h=10, Fig. 13(b) for 20, and Fig. 13(c) for 40, respectively. Here, ABCDEF correspond to the locations as can be seen in Fig. 4. In Fig. 13(a), α is about 1.5 kW/m^{2}K at the top of the first rib and decreases abruptly down to below 0.5 at its downstream side. Then, α recovers gradually as x/h increases and reaches 1.4 in the region of $4<x/h<8$, and also α decreases down to about 0.6 at the upstream side of the second rib and finally increases again at the top of the second rib. The average value of each α distribution in Fig. 13(a)~(c) decreases as p/h increases. This result may be explained in terms of the changes in the turbulence kinematic energy distributions among all ratios of p/h, as is pointed out in Fig. 9. Moreover, α between the square ribs for each p/h shows the largest value in the vicinity of x/h=5 as discussed in Fig. 12, where it can be evaluated as the reattachment point.

Figure 14 shows the Nusselt number (Nu) obtained from the heat transfer experiments by the square-ribbed fuel rods when p/h=10, 20 and 40 with Re. Here, local Nu and local Re are expressed respectively as: $Nu=q_w De/\lambda\,(T_w-\overline{T_b})$ and $Re=uDe/\nu$; Where, $\overline{T_b}$ is the average bulk temperature and u is the local axial velocity. Moreover, solid circle, open circle and solid triangle symbols represent the experimental data for p/h=10, 20 and 40 in the fully developed flow region. In addition, solid lines ($Nu_{p,t}$ and $Nu_{p,l}$) and broken lines ($Nu_{s,t}$, $Nu_{s,tr}$ and $Nu_{s,l}$) indicate the heat transfer empirical correlations in the spacer-ribbed annulus obtained from the previous experiment (Takase et al., 1993) and those of the concentric smooth annulus proposed by Dalle Donne and Meerwald (1973), Fujii, et al. (1980) and Kays and Crawford (1993). Here, the second suffixes of t, tr and l in Nu_p and Nu_s mean the turbulent, transitional and laminar, respectively. Each correlation was expressed by the following equations:

For the spacer-ribbed annulus,

$$Nu_{p,t} = 0.0219\,\mathrm{Re}^{0.8}\,\mathrm{Pr}^{0.4} \quad ; Re \geq 2000 \tag{15}$$

$$Nu_{p,l} = 7.0 \qquad ; Re \leq 1800 \tag{16}$$

For the concentric smooth annulus,

$$Nu_{s,t} = 0.018(Di/Do)^{-0.16}\,Re^{0.8}\,Pr^{0.4}\,; Re \geq 7000 \text{ [Dalle Donne and Meerwald (1973)]} \tag{17}$$

$$Nu_{s,tr} = 0.084(Re^{2/3} - 110)Pr^{0.4} \; ; 2700 < Re < 7000 \text{ [Fujii, et al. (1980)]} \tag{18}$$

$$Nu_{s,l} = 5.6 \quad ; Re \leq 2700 \text{ [Kays and Crawford (1993)]} \tag{19}$$

As shown in Fig. 14, although all Nusselt numbers with square-ribbed surfaces scattered widely, the following empirical correlation for the square-ribbed annulus was derived within an error of 15%.

$$Nu_r = 0.238(p/h)^{-0.45}\,Re^{0.68(p/h)^{0.0354}}\,Pr^{0.4} \; ; \; 10 \leq p/h \leq 40, \; 3000 \leq Re < 17000 \tag{20}$$

Here, Nu_r denotes the Nusselt number for the square-ribbed annulus.

For Re>3000, Nu_r is much higher than $Nu_{p,t}$ in ranges of $10 \leq p/h \leq 40$ and $3000 \leq Re < 17000$. In addition, the behavior of Nu_r is not similar to that of $Nu_{p,t}$. Though $Nu_{p,t}$ is reduced as a straight line as Re decreases in the region of Re<3000, Nu_r decreases suddenly as soon as Re drops to less than 3000. This characteristic resembles that of the concentric smooth annulus rather than that of the spacer-ribbed annulus. Regarding this point, the followings reason can be considered.

The h^+, defined by $h^+ = Uh/\nu$, is generally used as the roughness parameter. Here, U, h and ν denote the friction velocity, rib height and kinematic viscosity, respectively. Using h^+, every surface condition is divided into the following three regions (Cebeci et al., 1974); (a) $0 < h^+ < 4$ at the hydraulically smooth region, (b) $4 < h^+ < 70$ at the transitional region and (c) $70 < h^+$ at the fully rough region. For the region of $1000 \leq Re \leq 3000$ in this study, the roughness parameter of the square-ribbed annulus, h_r^+, is $30 \leq h_r^+ \leq 83.1$ for p/h=10, $27.4 \leq h_r^+ \leq 77$ for 20 and $22.4 \leq h_r^+ \leq 64$ for 40. Similarly, the roughness parameter of the spacer-ribbed annulus, h_p^+, is $129.3 \leq h_p^+ \leq 338.1$. For the change in Re from 3000 to 1000, the value of h_r^+ is reduced from the fully rough region to the transitional region and finally approaches the hydraulically smooth region. Therefore, it is expected that the effect of the turbulence promoter due to roughness decreases gradually with Re; however, the effect of the fluid viscosity increases. Namely, when Re was smaller, the surface of the square-ribbed annulus is close to the smooth wall. As

a consequence, Nu_r distributions will be characterized in the same way as those of a smooth annulus. On the other hand, when Re decreases from 3000 to 1000, the value of h_p^+ still stays in the fully rough region. Thus, the following consideration is concluded: For the spacer-ribbed annulus, since the turbulence effect by the spacer ribs has a strong influence even if Re is small, Nu_p shifts from the turbulent to laminar regions through a very small transitional region, maintaining the gradient of the turbulent region. In addition, since all prior studies by Maubach, Dalle Donne, etc. have been conducted under a Re range of more than 10000, no one pointed out these thermal-hydraulic characteristics of the square-ribbed annular channel under Re<10000.

A comparison of the predicted average Nusselt number (Nu_m) with the heat transfer empirical correlation expressed as Eq. (20) is shown in Fig. 15(a) for p/h=10, Fig. 15(b) for 20 and Fig. 15(c) for 40. Here, Nu_m is defined as:

$$Nu_m = q_w De / \lambda \left[\int_0^L (T_w - \overline{T_b}) dx / L \right] \tag{21}$$

where, L is the length of ABCDEF in Fig. 4 along the channel wall. All Nu_m are overestimated with the empirical correlation, however, a difference between the prediction and the empirical correlation is only 4~10% at p/h=10, 14~20% at 20, and 18~25% at 40, respectively. The heat transfer design for HTTR is thinking of the maximum permissible rate of ±25% for the heat transfer empirical correlation in a range of 3000≤Re<10000. Although the heat transfer prediction on the ribbed surface is in general very difficult so as to be influenced by the conditions of the near-wall flow field such as the size of the recirculation zone and the location and length of the reattachment point, the present predictions showed in relatively good agreement with the empirical correlation. It was concluded from these results that the heat transfer coefficients in the annular channel augmented by the square ribs were predicted numerically with sufficient accuracy regarding the engineering field under the conditions of helium coolant with high temperature and pressure and graphite heaters with the high radiation effect, and also the design study of the square-ribbed fuel rods for the nuclear reactors was able to conduct using the present numerical simulation.

5. CONCLUSIONS

Turbulent heat transfer characteristics in the square-ribbed annular fuel channel were analyzed numerically for the fully developed turbulent flow under the conditions of 3000≤Re≤20000 and 10≤p/h≤40. These results are summarized as follows:

(1) The detailed physical information in the square-ribbed annular fuel channel, such as local velocity, turbulence kinematic energy, temperature and heat transfer coefficient, were obtained from the present study. In particular, the size of recirculation zone and location of

a consequence, Nu_r distributions will be characterized in the same way as those of a smooth annulus. On the other hand, when Re decreases from 3000 to 1000, the value of h_p^+ still stays in the fully rough region. Thus, the following consideration is concluded: For the spacer-ribbed annulus, since the turbulence effect by the spacer ribs has a strong influence even if Re is small, Nu_p shifts from the turbulent to laminar regions through a very small transitional region, maintaining the gradient of the turbulent region. In addition, since all prior studies by Maubach, Dalle Donne, etc. have been conducted under a Re range of more than 10000, no one pointed out these thermal-hydraulic characteristics of the square-ribbed annular channel under Re<10000.

A comparison of the predicted average Nusselt number (Nu_m) with the heat transfer empirical correlation expressed as Eq. (20) is shown in Fig. 15(a) for p/h=10, Fig. 15(b) for 20 and Fig. 15(c) for 40. Here, Nu_m is defined as:

$$Nu_m = q_w De / \lambda \left[\int_0^L (T_w - \overline{T_b}) dx / L \right] \tag{21}$$

where, L is the length of ABCDEF in Fig. 4 along the channel wall. All Nu_m are overestimated with the empirical correlation, however, a difference between the prediction and the empirical correlation is only 4~10% at p/h=10, 14~20% at 20, and 18~25% at 40, respectively. The heat transfer design for HTTR is thinking of the maximum permissible rate of ±25% for the heat transfer empirical correlation in a range of 3000≤Re<10000. Although the heat transfer prediction on the ribbed surface is in general very difficult so as to be influenced by the conditions of the near-wall flow field such as the size of the recirculation zone and the location and length of the reattachment point, the present predictions showed in relatively good agreement with the empirical correlation. It was concluded from these results that the heat transfer coefficients in the annular channel augmented by the square ribs were predicted numerically with sufficient accuracy regarding the engineering field under the conditions of helium coolant with high temperature and pressure and graphite heaters with the high radiation effect, and also the design study of the square-ribbed fuel rods for the nuclear reactors was able to conduct using the present numerical simulation.

5. CONCLUSIONS

Turbulent heat transfer characteristics in the square-ribbed annular fuel channel were analyzed numerically for the fully developed turbulent flow under the conditions of 3000≤Re≤20000 and 10≤p/h≤40. These results are summarized as follows:

(1) The detailed physical information in the square-ribbed annular fuel channel, such as local velocity, turbulence kinematic energy, temperature and heat transfer coefficient, were obtained from the present study. In particular, the size of recirculation zone and location of

high temperature area after the square rib that were very important data from the viewpoint of heat transfer improvement of the square-ribbed fuel rods were also clarified.

(2) The difference between the predicted Nu_m and the empirical correlation expressed in Eq. (20) was within 10% for p/h=10, 20% for 20, and 25% for 40. It was concluded from this result that the augmented heat transfer coefficients augmented by the square ribs were predicted with sufficient accuracy under the conditions of helium coolant with high temperature and pressure and graphite heaters with the high radiation effect, and also the design study of the square-ribbed fuel rods for the nuclear reactors was able to conduct using the present numerical simulation.

(3) A large turbulence kinematic energy was generated at the upstream edge of the square rib where the flow impinged. When p/h=10, the turbulence with large kinematic energy always existed in the channel. However, when p/h=40, the large turbulence produced at the square rib decreased along the flow direction and disappeared when it approached the next rib. From a reason which the heat transfer coefficient is in general augmented with the strength of turbulence, it was found that the heat transfer coefficients in the square-ribbed annular fuel channel with the larger p/h were lower than that with the smaller p/h.

(4) Regarding the present experimental results in Fig. 14, Nu_r distribution for each p/h showed the feature of the transitional region in $1000<Re<3000$, such as seen in case of the smooth annulus. As a result of this, it was considered that the value of h_r^+ was reduced as Re decreased and approached the value of the hydraulically smooth region. On the other hand, the turbulent heat transfer in $Re \geq 3000$ was correlated well using Eq. (20) in $3000 \leq Re < 17000$. Regarding the rib-roughened narrow annulus, the heat transfer characteristics in the low turbulent region of $Re<10000$ were first clarified by the present experimental results.

ACKNOWLEDGMENTS

The author would like to express his sincere gratitude to Mr. Akino, who is a chief of the nuclear heat utilization engineering laboratory in JAERI, for his very helpful suggestions regarding the present study. The FLUENT code was provided by Ryutai Consultant Co., Ltd. in Japan. The author would like to express his thanks to Mr. Mouri who is the president of the company.

high temperature area after the square rib that were very important data from the viewpoint of heat transfer improvement of the square-ribbed fuel rods were also clarified.

(2) The difference between the predicted Nu_m and the empirical correlation expressed in Eq. (20) was within 10% for p/h=10, 20% for 20, and 25% for 40. It was concluded from this result that the augmented heat transfer coefficients augmented by the square ribs were predicted with sufficient accuracy under the conditions of helium coolant with high temperature and pressure and graphite heaters with the high radiation effect, and also the design study of the square-ribbed fuel rods for the nuclear reactors was able to conduct using the present numerical simulation.

(3) A large turbulence kinematic energy was generated at the upstream edge of the square rib where the flow impinged. When p/h=10, the turbulence with large kinematic energy always existed in the channel. However, when p/h=40, the large turbulence produced at the square rib decreased along the flow direction and disappeared when it approached the next rib. From a reason which the heat transfer coefficient is in general augmented with the strength of turbulence, it was found that the heat transfer coefficients in the square-ribbed annular fuel channel with the larger p/h were lower than that with the smaller p/h.

(4) Regarding the present experimental results in Fig. 14, Nu_r distribution for each p/h showed the feature of the transitional region in $1000<Re<3000$, such as seen in case of the smooth annulus. As a result of this, it was considered that the value of h_r^+ was reduced as Re decreased and approached the value of the hydraulically smooth region. On the other hand, the turbulent heat transfer in $Re \geq 3000$ was correlated well using Eq. (20) in $3000 \leq Re < 17000$. Regarding the rib-roughened narrow annulus, the heat transfer characteristics in the low turbulent region of $Re<10000$ were first clarified by the present experimental results.

ACKNOWLEDGMENTS

The author would like to express his sincere gratitude to Mr. Akino, who is a chief of the nuclear heat utilization engineering laboratory in JAERI, for his very helpful suggestions regarding the present study. The FLUENT code was provided by Ryutai Consultant Co., Ltd. in Japan. The author would like to express his thanks to Mr. Mouri who is the president of the company.

REFERENCES

A. Acharya, S. Dutta, T. A. Myrum, and R. S. Baker, Periodically developed flow and heat transfer in a ribbed duct, Int. J. Heat Mass Transfer, 36, 8(1993)2069-2082.

T. Cebeci and A.M. O. Smith, Analysis of Turbulent Boundary Layer, Applied Mathematics and Mechanics, Academic Press, New York, (1974)130.

B. H. Chang, and A. F. Mills, Turbulent flow in a channel with transverse rib heat transfer augmentation, Int. J. Heat Mass Transfer, 36, 6, (1993)1495-1469.

M. Dalle Donne, and L. Meyer, Turbulent convective heat transfer from rough surfaces with two dimensional rectangular ribs, Int. J. Heat Mass Transfer, 20, (1977)583-620.

S. Fujii, M. Hishida, H. Kawamura, and N. Akino, Heat transfer in annular channels under the high heat flux conditions, 17the Japan Heat Transfer Symposium, A213(1980)97-99.

A, Goldsmith, T. E. Waterman, and H. J. Hirschborn, Handbook of Thermophysical Properties of Solid Materials: Vol.1, MACMILLAN, New York, (1961)127-131.

J. C. Han, L. R. Glicksman, and W. M. Rohsenow, An investigation of heat transfer and friction for rib-roughened surfaces, Int. J. Heat Mass Transfer, 21, (1978)1143-1156.

M. Hishida and K. Takase, Heat transfer coefficient of the ribbed surface, Proceedings of ASME/JSME Thermal Engineering, 3, (1991)103-110.

W. P. Jones, and B. E. Launder, The prediction of laminarization with a two-equation model of turbulence, Int. J. Heat Mass Transfer, 15, (1972)301-314.

W. M. Kays and M. E. Crawford, Convective heat and mass transfer (third edition), McGRAW-HILL, New York, (1993)123.

B. E. Launder, and D. B. Spalding, The numerical computation of turbulent flows, Computer Methods in Applied Mechanics and Engineering, 3, (1974)269-289.

T. M. Liou, J. J. Hwang, and S. H. Chen, Turbulent heat transfer and fluidflow in a channel with repeated rib pairs, Proc. of ASME/JSME Thermal Eng., 3,(1991)205-212.

B. K. Lee, N. H. Cho, and Y. D. Choi, Analysis of periodically fully developed turbulent flow and heat transfer by k-ε equation model in artificially roughened annulus, Int. J. Heat Mass Transfer, 31, (1988)1797-1806.

T. Makino, T. Kunitomo, and T. Mori, Study on characteristics of thermal radiation of heat resisting alloy with high temperature, J. Japan Society Mechanical Engineering, 49, 441(1983)1040-1047.

K. Maubach, Rough annulus pressure drop - Interpretation of experiments and recalculation for spacer ribs, Int. J. Heat Mass Transfer, 15, (1972)2489-2498.

K. Takase, S. Maruyama, R. Hino, M. Hishida, N. Izawa, and H. Shimomura, Experimental studies on thermal and hydraulic performance of fuel stack on VHTR, (I) Test results of HENDEL single-channel test rig with uniform heat flux distribution, J. Atomic Energy Society of Japan, 28, 5(1986)428-435.

K. Takase, R. Hino, and Y. Miyamoto, Thermal and hydraulic tests of standard fuel rod of HTTR with HENDEL, J. Atomic Energy Society of Japan, 32, 11(1990)1107-1110.

K. Takase, R. Hino, and Y. Miyamoto, Heat transfer and fluid dynamics of high heat flux fuel rod for HTTR : Heat transfer augmentation by square ribbed surface, J. Atomic Energy Society of Japan, 33, 10(1991)975-982.

K. Takase, R. Hino, and Y. Miyamoto, Thermal and hydraulic performances of fuel rods with transverse square ribs in HTTR, J. Atomic Energy Society of Japan, 35, 11(1993)996-998.

K. Takase, Experimental and analytical studies on turbulent heat transfer performance of a fuel rod with spacer ribs for high temperature gas-cooled reactors, Nucl. Eng. Des., 154, (1995)345-356.

K. Takase and N. Akino, Numerical simulation on thermal-hydraulic cheracteristics in annular fuel channel with spacer ribs, 30th Intersociety Energy Conversion Engineering Conference, 2, (1995)645-650.

S. V. Patankar, C. H. Liu, and E. M. Sparrow, Fully developed flow and heat transfer in ducts having streamwise-periodic variations of cross-sectional area, J. Heat Transfer, 99(1977)180-186.

S. V. Patankar, Numerical Heat Transfer and Fluid Flow, McGRAW-HILL, New York, (1980)130-136.

NOMENCLATURE

A : van Driest constant

C_μ, C_1, C_2 : turbulence model constants, respectively

Di : fuel rod diameter

Do : outer channel diameter

De : hydraulic diameter

E : log-law constant

H : channel height =De/2

h : square-rib height

k : turbulence kinematic energy

L : axial length

Nu : Nusselt number

P : pressure

p : square-rib pitch

Pr, Pr_t : Prandtl number, turbulent Prandtl number

q_w : wall heat flux

Re : Reynolds number =uDe/ν

T : temperature

T_w, T_b : inner wall and bulk temperatures

u, v : axial and radial velocities

U : friction velocity

w : square-rib width

x, r : axial and radial coordinates

y : distance from the wall

y^+ : dimensionless distance

Greek symbols

ε : dissipation

κ : von Karman's constant

λ : thermal conductivity

μ, μ_t : viscosity, turbulent viscosity

ν : kinematic viscosity

ρ : density

σ_k , σ_ε : turbulent Prandtl number for k and ε

τ_w : wall shear stress

Suffixes

p : spacer-ribbed annulus

r : square-ribbed annulus

s : concentric smooth annulus

t, tr, l : turbulent, transitional and laminar

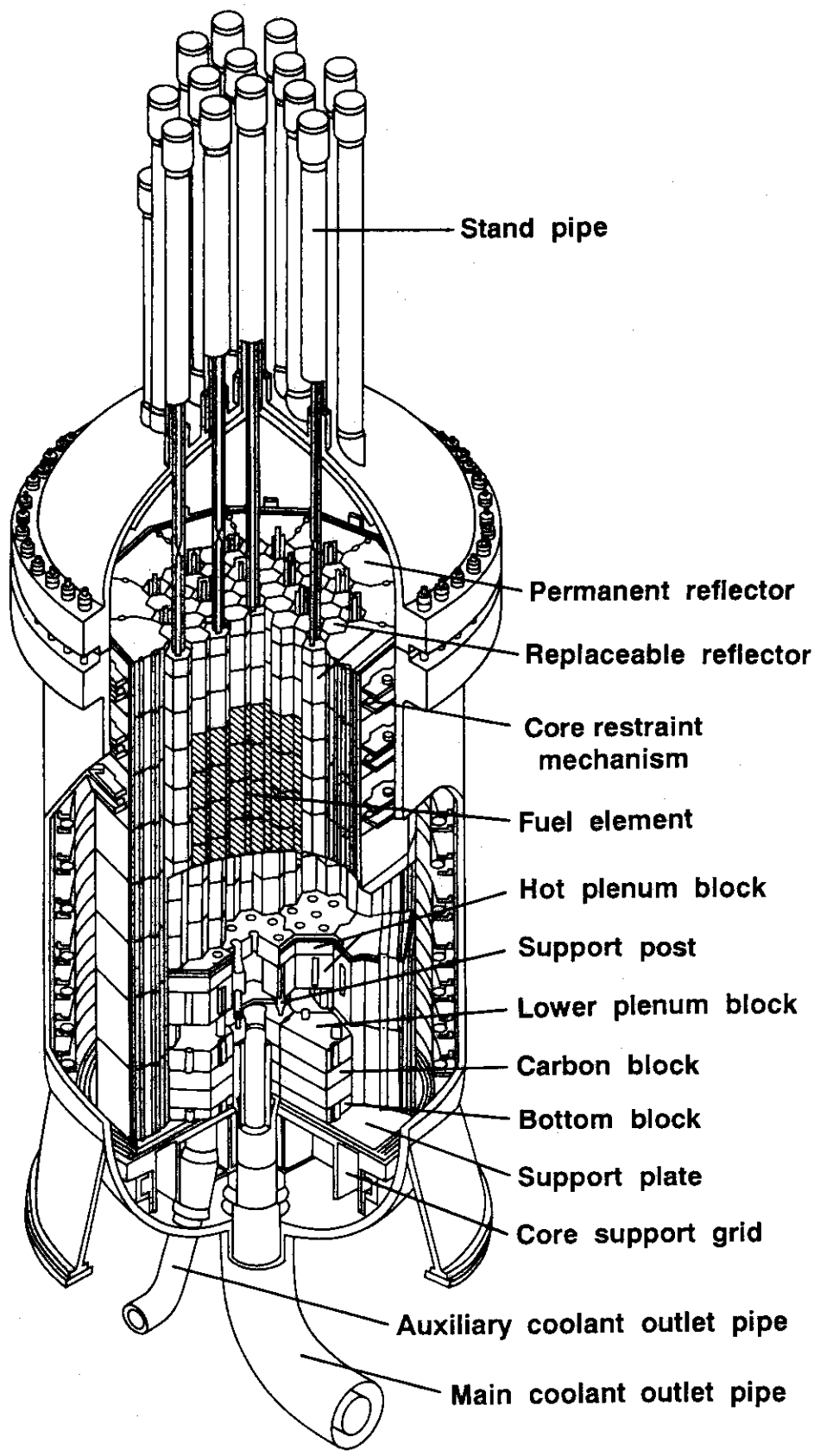

Fig. 1 Structural drawing in the HTTR pressure vessel: Helium gas flows downward through the reactor core consisting of many fuel elements shown as a hatched area.

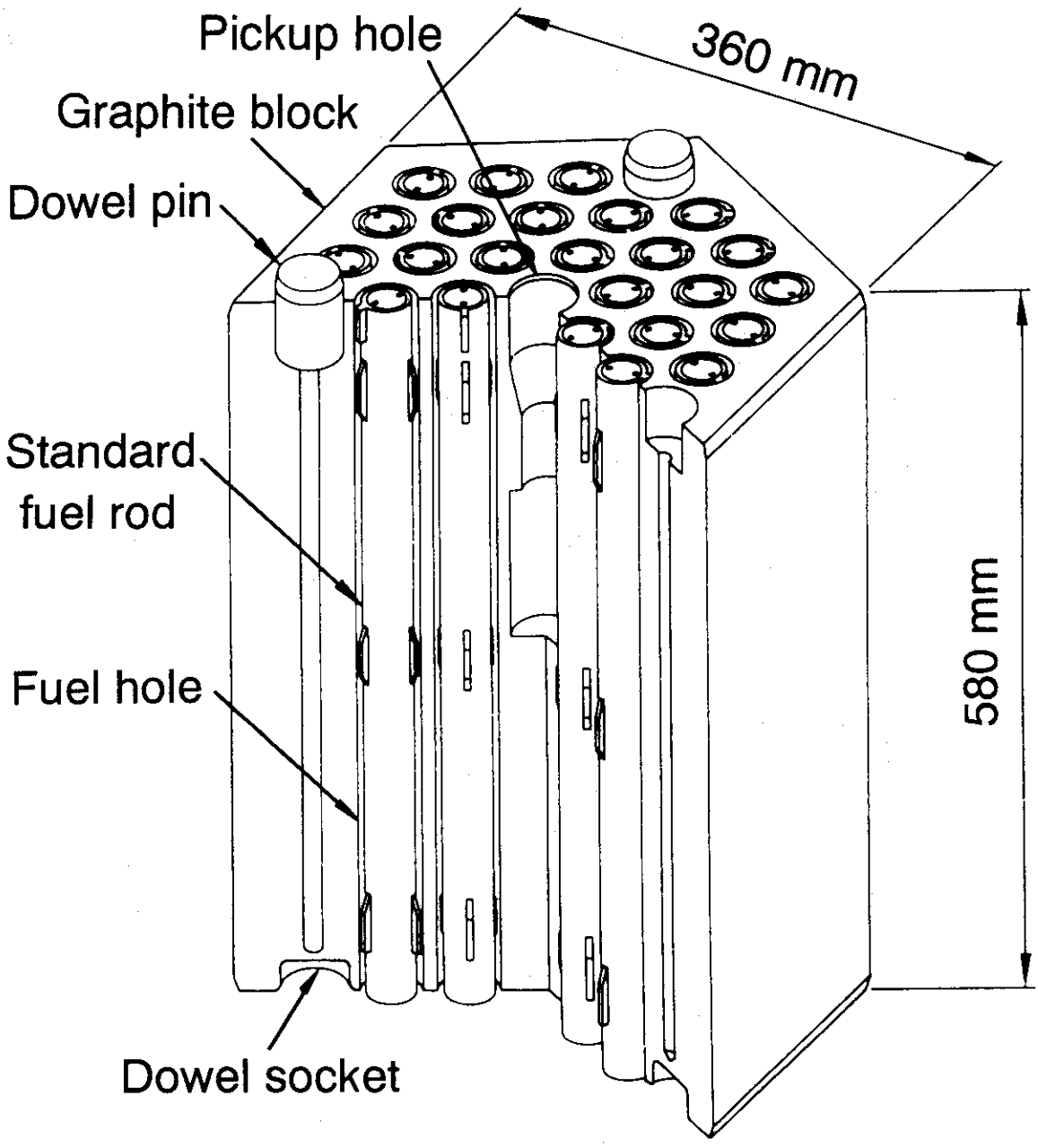

Fig. 2 Schematic of the HTTR fuel element consisted of a hexagonal graphite block and 33 standard fuel rods with three-dimensional spacer ribs: Helium gas flows downward through the annular channels between the fuel hole with a diameter of 41 mm and the fuel rod with an external diameter of 34 mm.

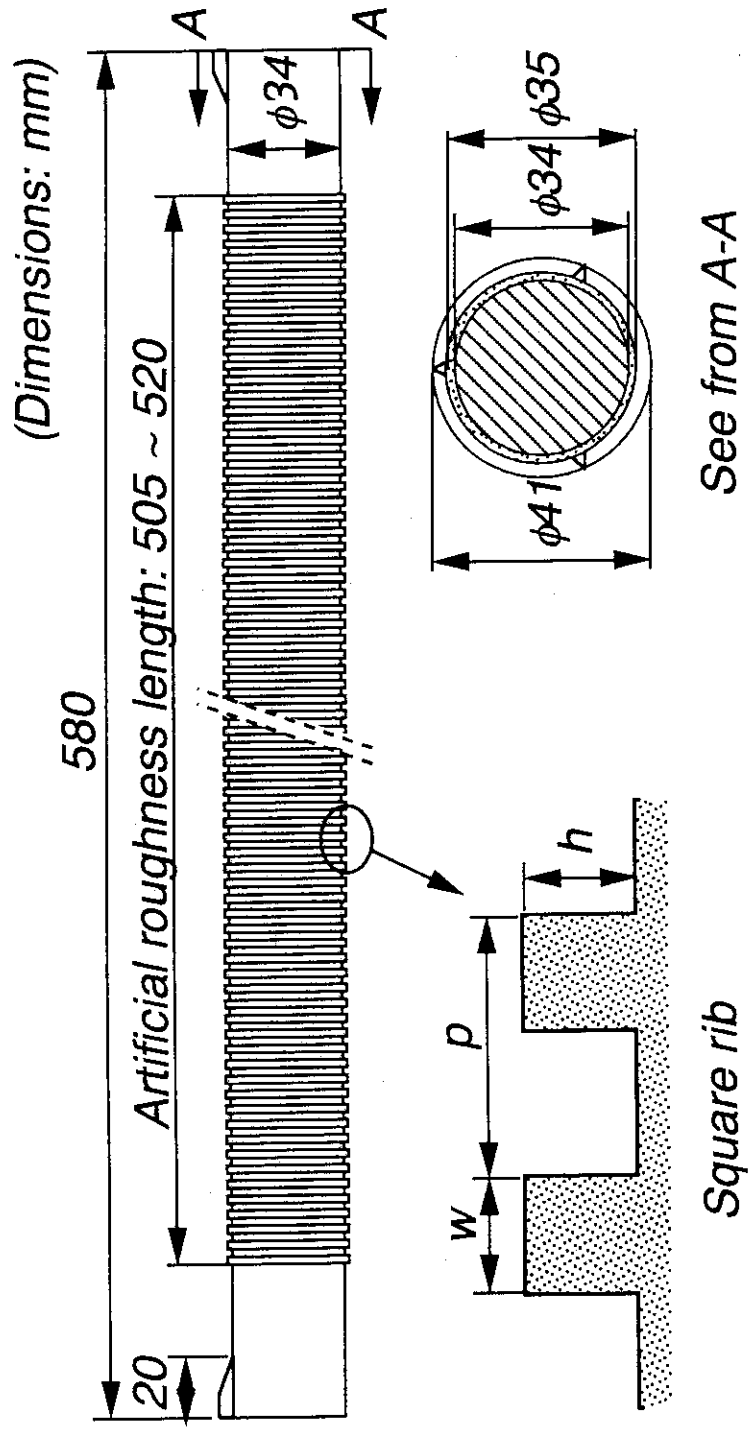

Fig. 3 Configurations of a square-ribbed fuel rod and square ribs.

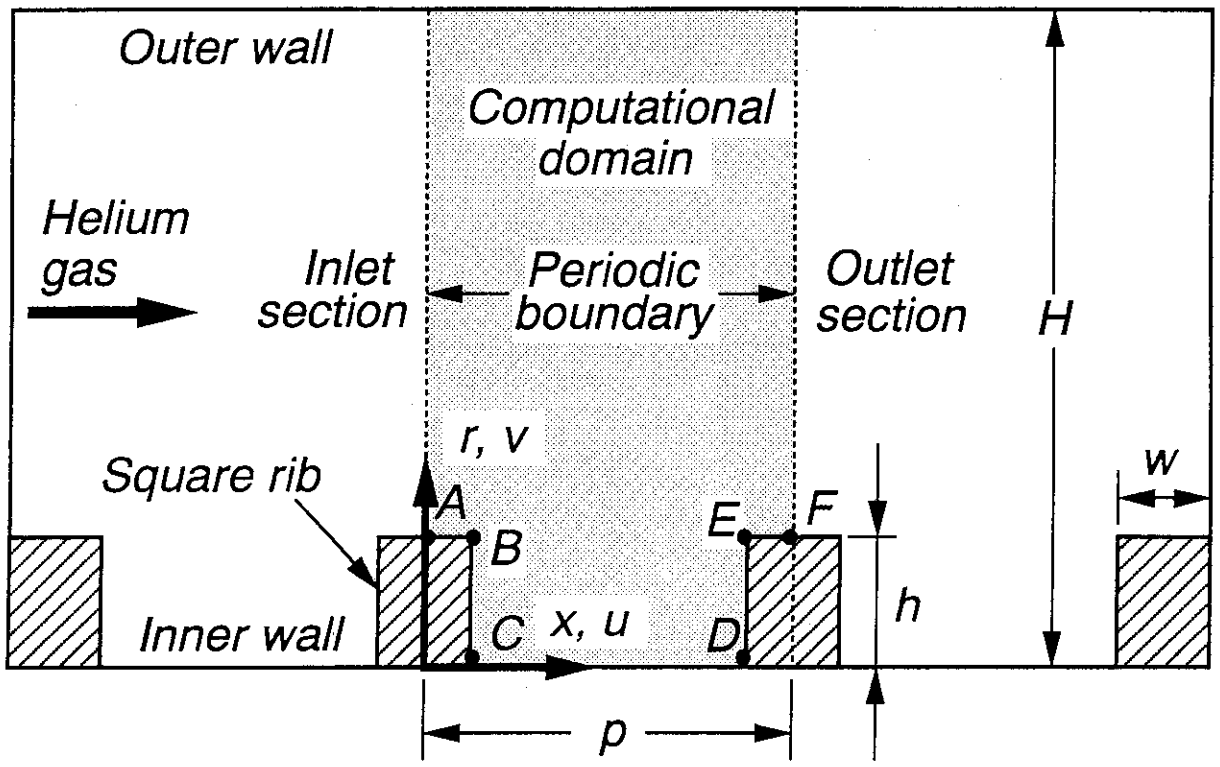

Fig. 4 Analytical model and boundary conditions for a turbulent flow over repeated transverse square ribs in a two-dimensional axisymmetrical coordinate.

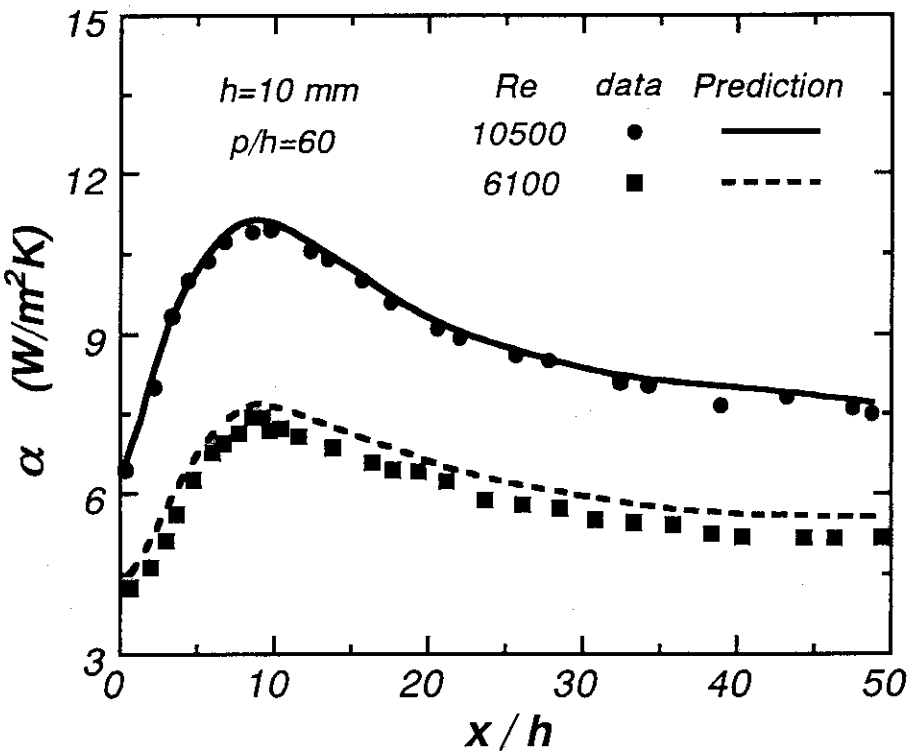

Fig. 5 Comparison of the predicted heat transfer coefficients with the experimental data in a rectangular channel with the square-ribbed lower wall.

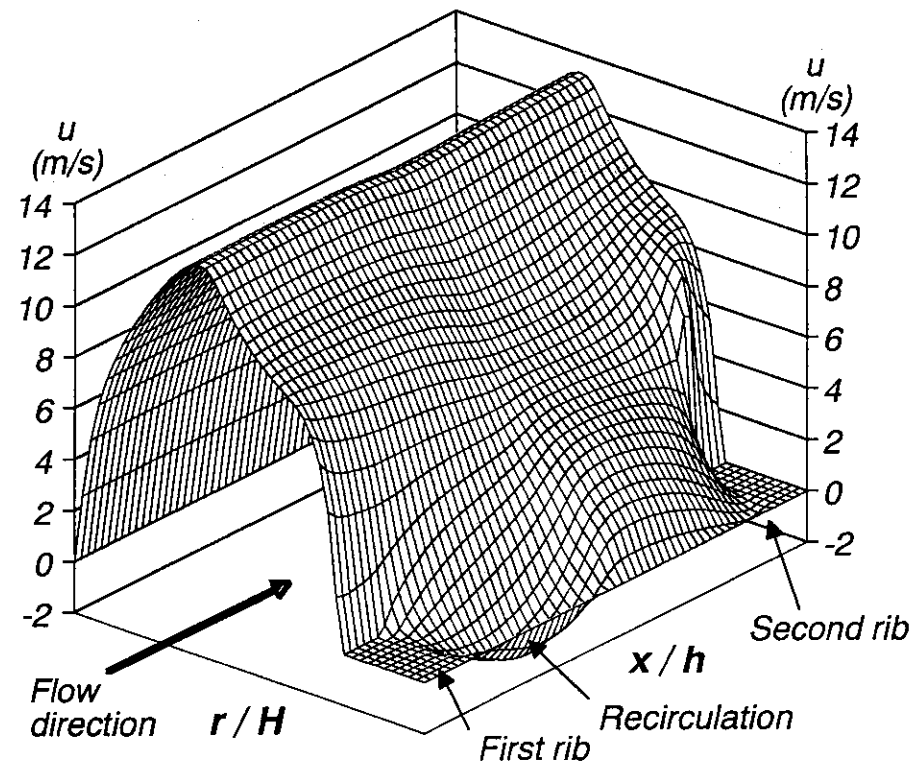

Fig. 6 The predicted axial velocity distribution along the flow direction between a couple of square ribs at p/h=10 and Re=5000.

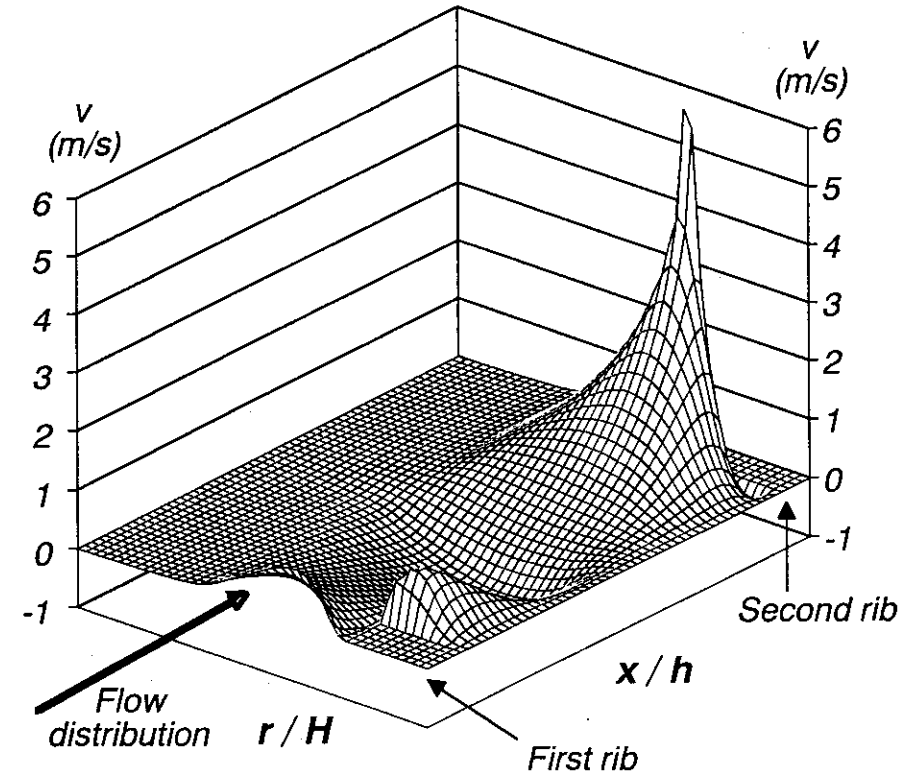

Fig. 7 The predicted radial velocity distribution along the flow direction between the square ribs at p/h=10 and Re=5000.

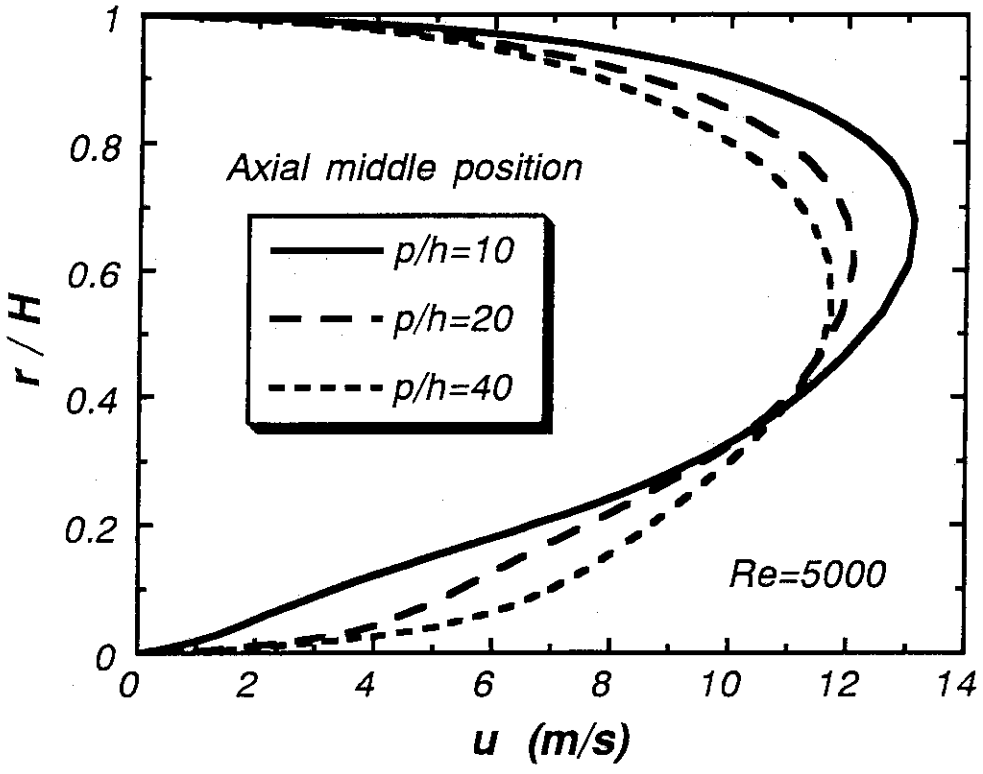

Fig. 8 The predicted axial velocity profiles at the axial middle position between the square ribs at Re=5000 when p/h=10, 20 and 40.

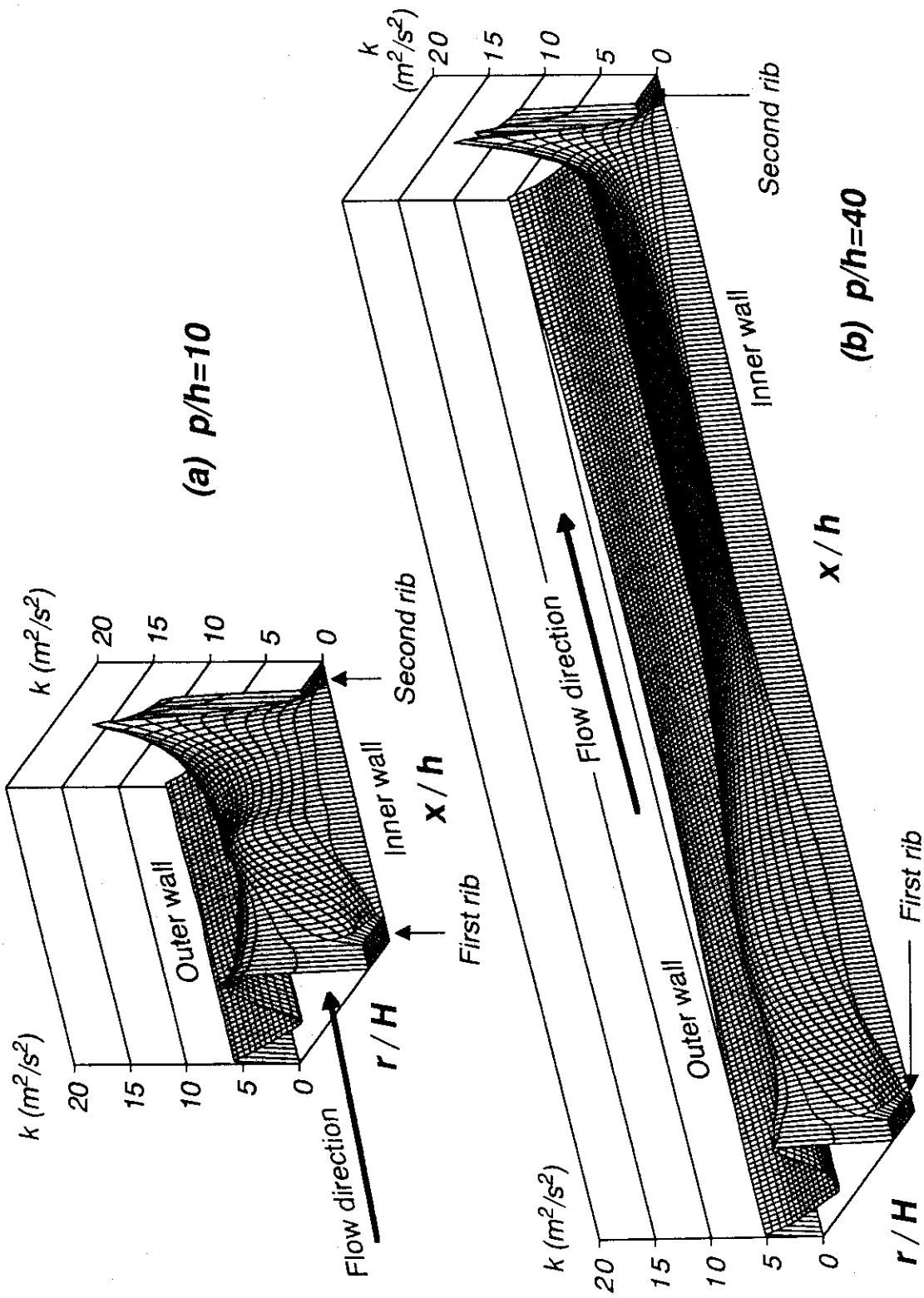

Fig. 9 The predicted turbulence kinematic energy distributions along the flow direction between the square ribs at Re=5000 when p/h=10 and 40.

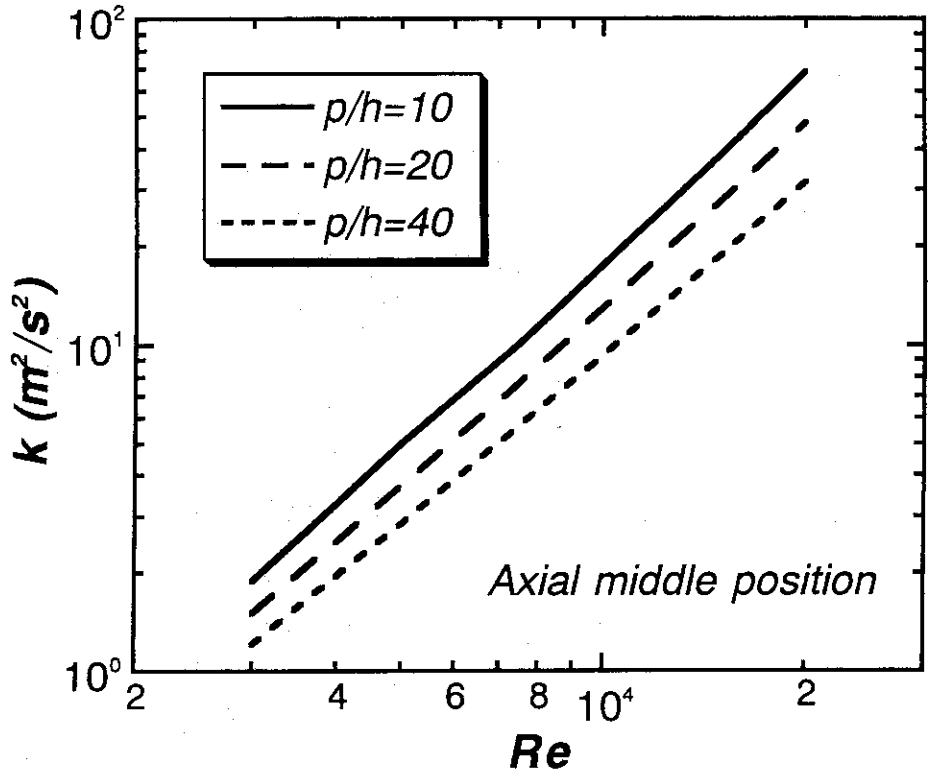

Fig. 10 Distributions of the predicted maximum turbulence kinematic energy at the axial middle position with Re when p/h=10, 20 and 40.

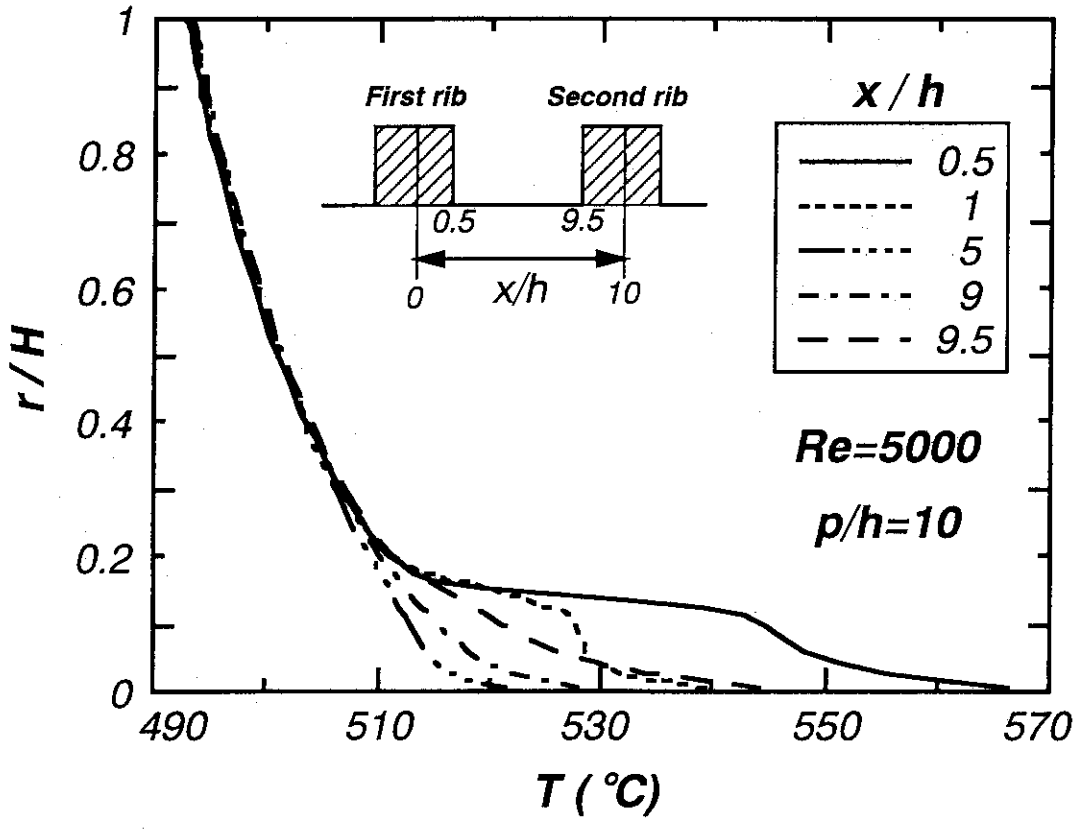

Fig. 11 The predicted radial temperature profiles between the inner and outer walls with different ratios of x/h at p/h=10 and Re=5000.

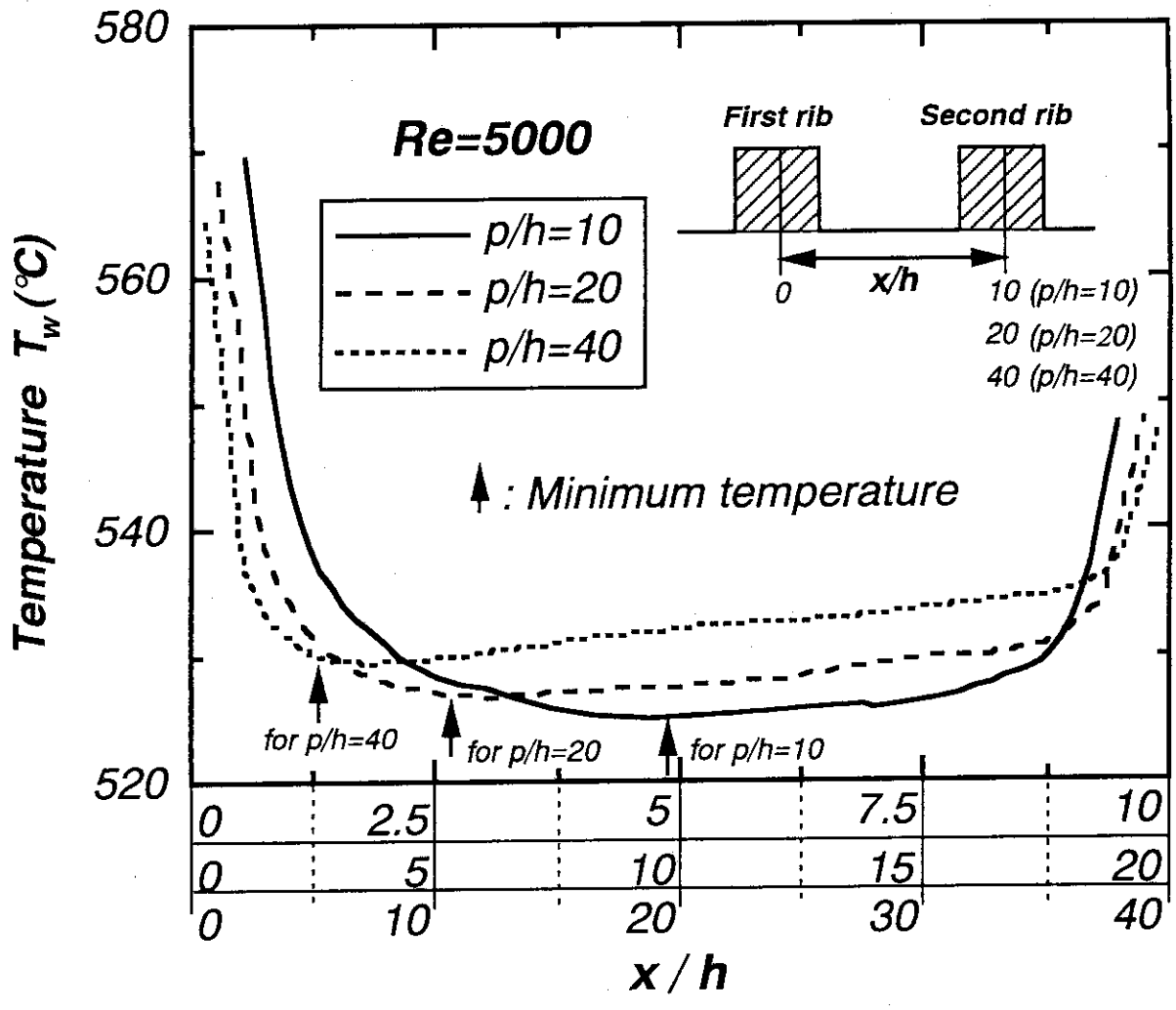

Fig. 12 The predicted inner wall temperature distributions between the square ribs with different ratios of p/h at Re=5000.

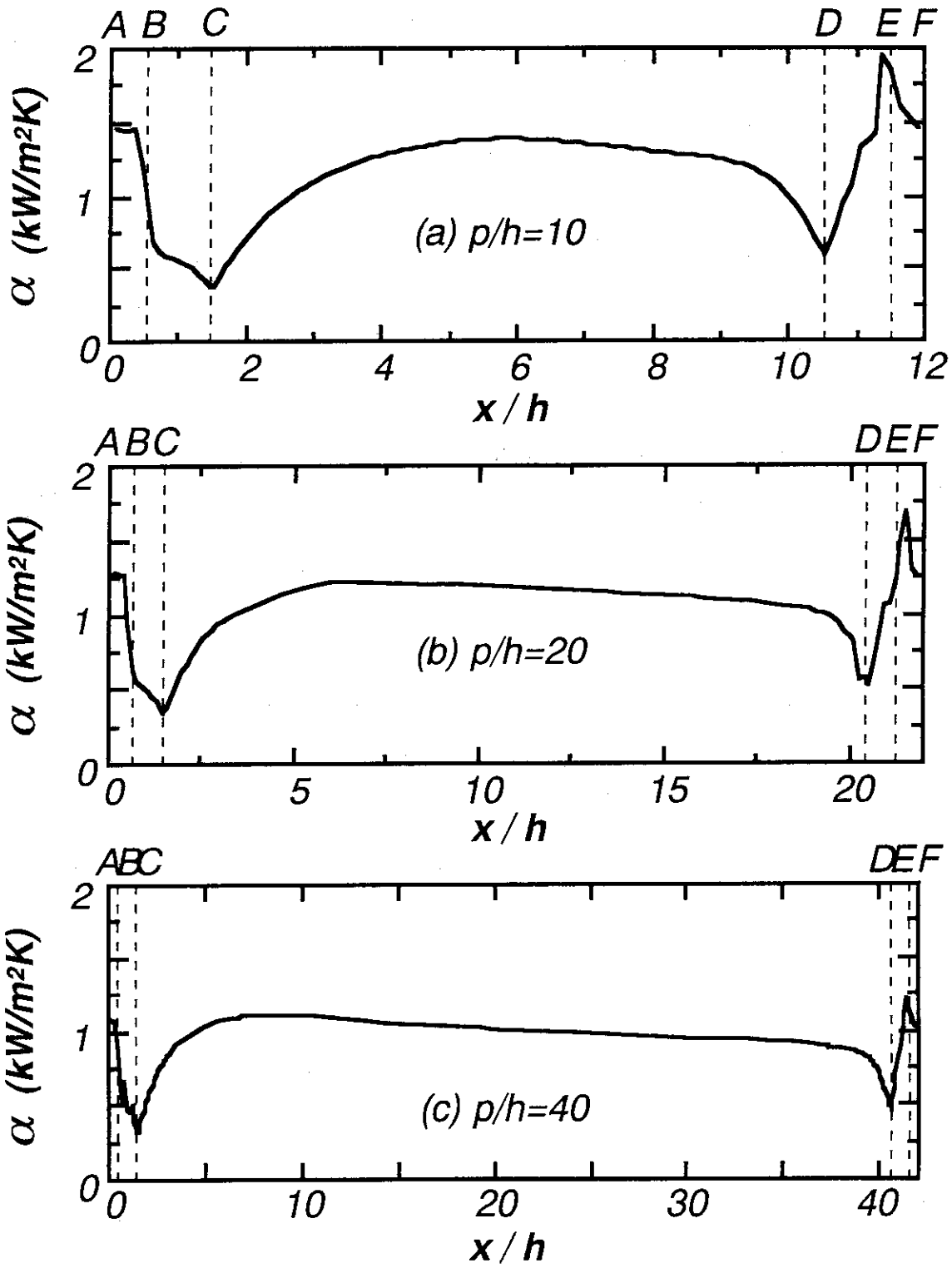

Fig. 13 The predicted local heat transfer coefficient distributions along the flow direction at Re=5000 when p/h=10, 20 and 40.

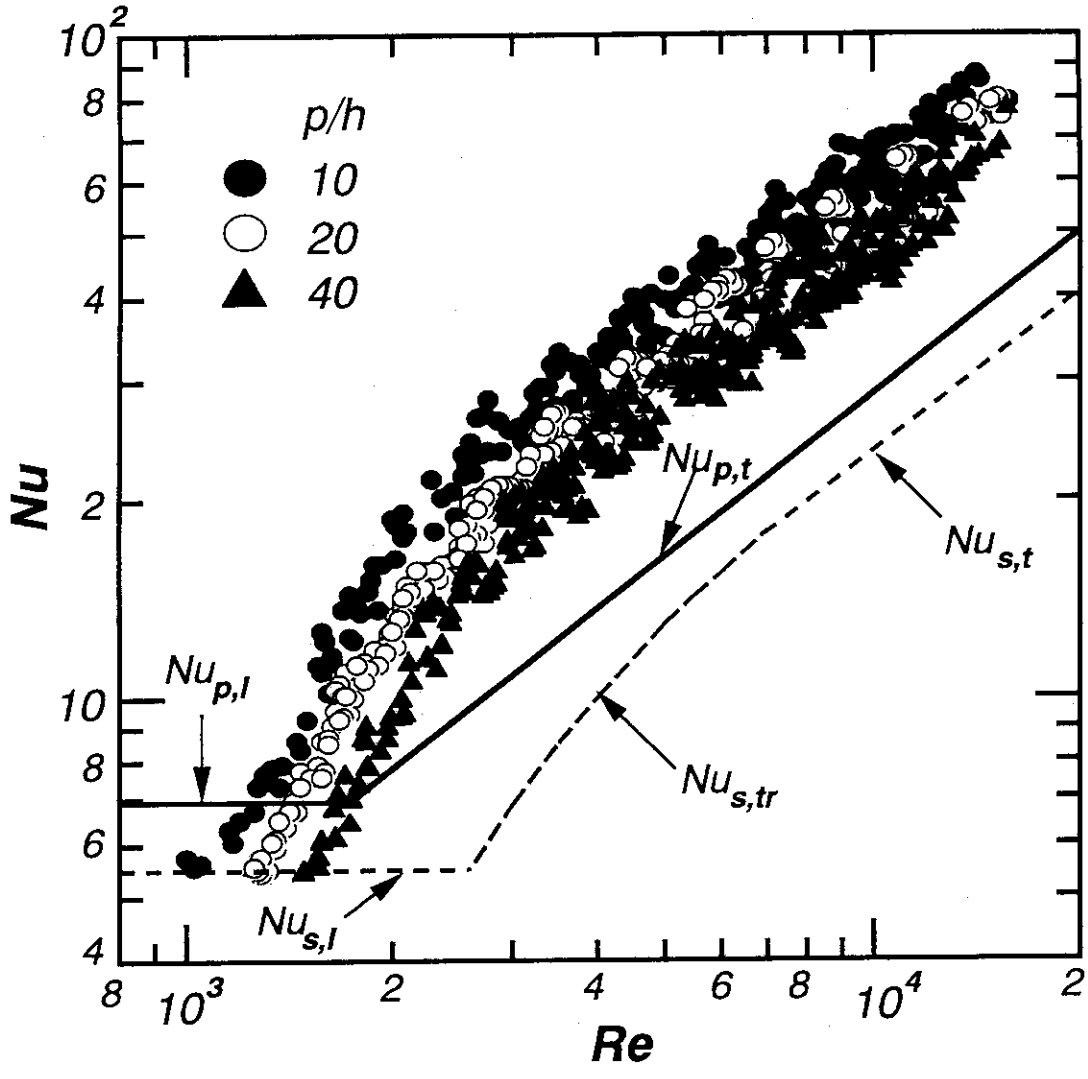

Fig. 14 Variation in Nusselt number obtained from the experimental data of the square-ribbed fuel rods when p/h=10, 20 and 40 with Re:Where, solid circle, open circle and solid triangle symbols represent the experimental data for p/h=10, 20 and 40; Solid lines for Nu_p and broken lines for Nu_s mean the empirical correlations for the spacer-ribbed annulus and concentric smooth annulus, respectively; Subscripts of t, tr and l show turbulent, transition and laminar region, respectively.

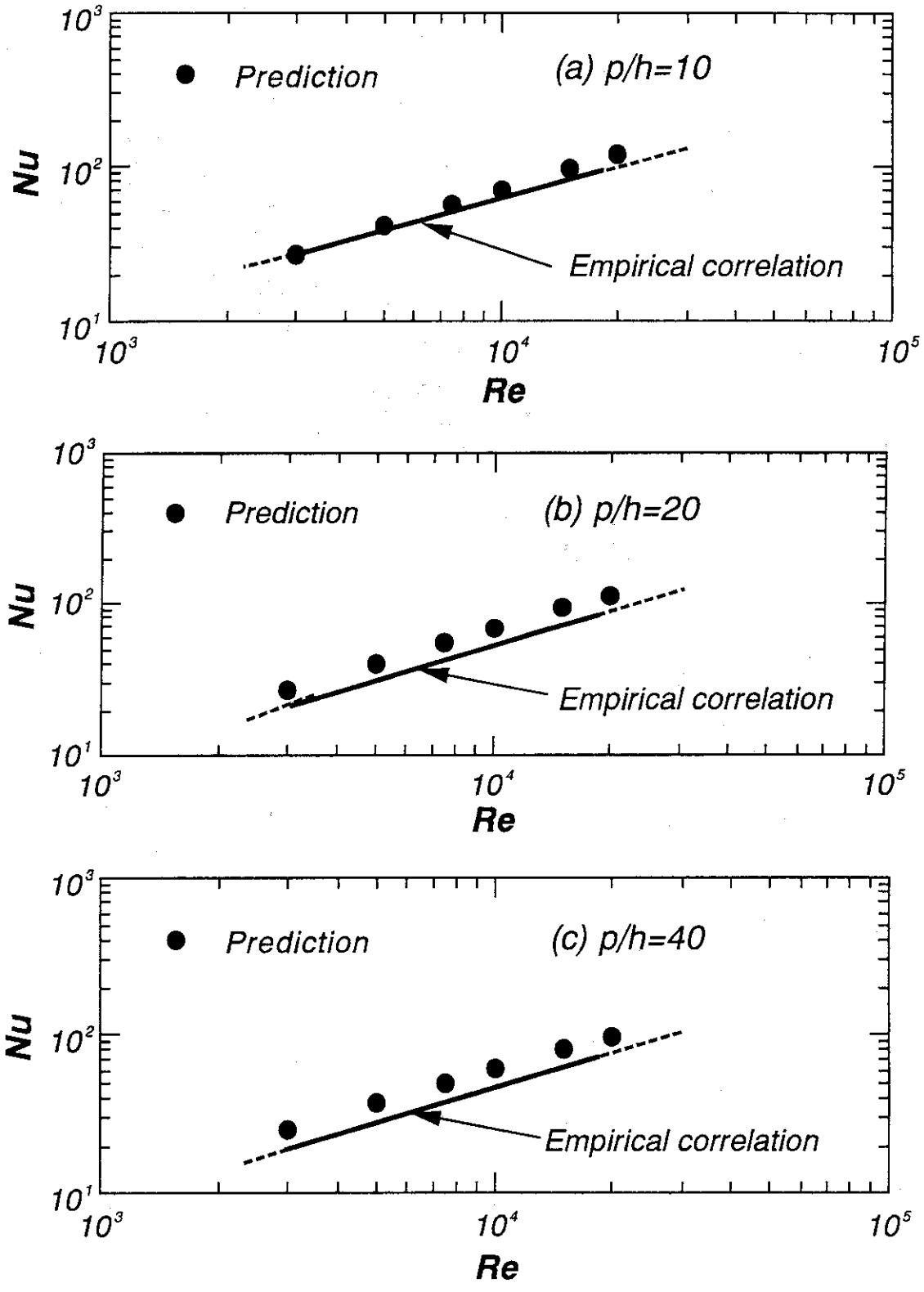

Fig. 15 Comparison of the predicted average Nusselt number with the heat transfer empirical correlation when p/h=10, 20 and 40.